

A Projectional Ansatz to Reconstruction

Sören Dittmer

Center for Industrial Mathematics (ZeTeM)
University of Bremen, Germany
soeren.dittmer@gmail.com

Peter Maass

Center for Industrial Mathematics (ZeTeM)
University of Bremen, Germany
pmaass@uni-bremen.de

Abstract

Recently the field of inverse problems has seen a growing usage of mathematically only partially understood learned and non-learned priors. Based on first principles we develop a projectional approach to inverse problems which addresses the incorporation of these priors, while still guaranteeing data consistency. We implement this projectional method (PM) on the one hand via very general Plug-and-Play priors and on the other hand via an end-to-end training approach. To this end we introduce a novel alternating neural architecture, allowing for the incorporation of highly customized priors from data in a principled manner. We also show how the recent success of Regularization by Denoising (RED) can, at least to some extent, be explained as an approximation of the PM. Furthermore we demonstrate how the idea can be applied to stop the degradation of Deep Image Prior (DIP) reconstructions over time.

1 Introduction

Recently the field of inverse problems has seen a growing usage of mathematically only partially understood learned (e.g. Lunz et al. [2018], Adler and Öktem [2018], Hauptmann et al. [2018], Yang et al. [2018], Bora et al. [2017]) and non-learned (e.g. Venkatakrishnan et al. [2013], Romano et al. [2017], Ulyanov et al. [2018], Veen et al. [2018], Mataev et al. [2019], Dittmer et al. [2018]) priors.

A key challenge of many of these approaches, especially the learned ones, lies in the fact that it is often hard or even impossible to guarantee data consistency for them i.e. that the reconstruction is consistent with the measurement. More formally: Given a continuous forward operator A and a noisy measurement $y^\delta := y + \eta = Ax + \eta$, where η some noise, could a computed reconstruction x^\dagger have created the measurement y^δ , given the noise level $\|\eta\|$. We call the set of reconstructions that fulfill this property the **set of valid solutions** and denote it by $V(A, y^\delta, \|\eta\|)$.

In this paper we present an approach to reconstruction problems that guarantees data consistency by design. We start by reexamining the core challenge of reconstruction problems. We then use the gained insights to propose the projectional method (PM) as a very general framework to tackle inverse problems. A key challenge of the PM lies in the calculation of the projection into the set of valid solutions, V . We analyze V and derive a projection algorithm to calculate

$$P_V x^* = \arg \min_{x \in V} \|x - x^*\|, \quad (1)$$

for A being a linear continuous operator. This class of operators includes a wide variety of forward operators like blurring, the Radon transform which plays a prominent role in medical imaging, denoising (the identity), compressed sensing, etc., see e.g. Engl et al. [1996], Eldar and Kutyniok [2012]. We also compute the derivative, ∂P_V , of P_V via the implicit function theorem, thereby allowing for the usage of P_V as a layer within an end-to-end trained model.

We then, in Section 3, demonstrate how the PM not only compares to the recently proposed Regularization by Denoising (RED) (Romano et al. [2017]), but also how RED can be seen as a relaxation

of PM. In Section 4 we demonstrate how one can apply the projectional approach to Deep Image Prior (DIP) (Ulyanov et al. [2018]) to avoid the often observed degradation of its reconstructions over time, alleviating the need for early stopping. Finally, in Section 5, we present a novel neural network architecture based on the PM. The architecture allows for a principled incorporation of prior knowledge from data, while still guaranteeing data consistency – despite an end-to-end training. Summary of contributions in order:

- A projectional approach to reconstruction that guarantees data consistency.
- The derivation of a neural network layer that projects into the set of valid solutions.
- Interpretation of RED as an approximation to the projectional method (PM).
- Numerical comparison/application of the approach to RED and DIP.
- A novel neural network architecture that allows for a principled incorporation of prior knowledge, while still guaranteeing data consistency.

2 A Projectional Ansatz

2.1 Motivation and Idea

We begin with some definitions and notation which we will use throughout the paper:

- Let X and Y denote real Hilbert spaces and $A : X \rightarrow Y$ a continuous linear operator.
- For a given $x \in X$ we define $y := Ax$.
- Let further $\delta > 0$ be a given **noise level** and $y^\delta := y + \eta$ be a noisy measurement, where the classical assumption is $\|\eta\| \leq \delta$ with η some random noise (Engl et al. [1996]).
- Let $U \subset X$ be a non-empty set, called the **set of plausible solutions** (e.g. sparse or smooth elements or even natural images). For all measurements we will assume $x \in U$.
- As discussed above, we informally define the **set of valid solutions** as the set $V \subset X$ such that the elements of $V(A, y^\delta, \delta)$ would “explain” the measurement y^δ , given the operator A and the noise level δ . A formal discussion will follow in Section 2.2.

Given these definitions we can define the central object of this paper: the set $V \cap U$, which we call the set of **valid and plausible** solutions. The main goal of this paper is to find an element of $V \cap U$, which we assume to be non-empty.

If we assume U and V to be closed and convex or to have one of many much weaker properties, see Gubin et al. [1967], Bauschke and Borwein [1993], Lewis and Malick [2008], Lewis et al. [2009], Drusvyatskiy et al. [2015], etc., we can use **von Neumann’s alternating projection algorithm** (Bauschke and Borwein [1993]) to accomplish the task of finding an element in $V \cap U$. The algorithm is given by the alternating projections into the two sets V and U and returns in a point in their intersection, i.e.

$$U \cap V \ni P_V \circ P_U \circ P_V \circ P_U \circ \dots \circ P_V x_0, \quad (2)$$

for all $x_0 \in X$, we always simply set $x_0 = 0$. For a visual representation of the algorithm see Figure 6 in the appendix. In this paper we use this alternating pattern to tackle reconstruction problems. Therefore we rely on having the projections P_V and P_U . Since P_U is task dependent, we begin by analyzing the set of valid solutions and its projection P_V .

2.2 The Set of Valid Solutions

In this subsection we motivate a definition of the set of valid solutions and analyze it. The classical assumption for inverse problems is that one has $\|\eta\| \leq \delta$ for some noise η and a noise level $\delta > 0$. This could motivate the definition of the set of valid solutions as

$$\bar{V}(A, y^\delta, \delta) := \{x \in X : \|Ax - y^\delta\| \leq \delta\}. \quad (3)$$

But, considering the fact that η is usually assumed to be “unstructured noise” (e.g. Gaussian) and X is usually assumed to be high- (e.g. images) or even infinite-dimensional (e.g. functions), we can

utilize the principle of concentration of measure (Talagrand [1996]) to conclude that $\|\eta\| \approx \delta$, with increasing accuracy for higher dimensions. This motivates us to define

$$V(A, y^\delta, \delta) := \{x \in X : \|Ax - y^\delta\| = \delta\}. \quad (4)$$

Note that this set is closed and convex since A is continuous. Furthermore, since A is linear, \bar{V} is also convex. This makes a projection onto \bar{V} well defined, as well as onto V up to a null set. We can rewrite the set V as

$$V = \left\{ x \in X : (x - y^\delta)^T \frac{A^T A}{\delta^2} (x - y^\delta) = 1 \right\}, \quad (5)$$

where $\frac{A^T A}{\delta^2}$ is positive semidefinite. If $\frac{A^T A}{\delta^2}$ was a positive definite operator V could be characterized by a hyperellipsoid. The "semi-" causes it to be a product space $E \times W$ of a $\text{rank}(A)$ -dimensional hyperellipsoid $E \subset X$ with a nullity(A)-dimensional vector space $W \subset X$ – think of an elliptical $\text{rank}(A)$ -dimensional cookie cutter cutting a $\dim(X)$ -dimensional cookie, for an illustration see Figure 7 in the appendix.

We now discuss how to calculate the projection P_V and turn it into a neural network layer.

2.3 Projection into the Valid Solutions as a Layer

In this subsection we first discuss how to calculate P_V and then how to calculate its derivative. The calculation of its derivative is of interest, since we want to use the projection within a neural network. It would not be feasible to calculate the derivative via some automatic differentiation package, since the calculation of the projection is iterative, which could quickly cause the process to exceed the memory of the machine.

We begin by deriving an algorithm to calculate the projection into V i.e. how to solve the constrained optimization problem given by Expression (1). We can use the method of Lagrangian multipliers to rewrite the expression as the optimization problem

$$P_V x^* := \arg \min_{x \in X} L_{\mu(\delta, x^*)}(x^*, x), \quad (6)$$

where

$$L_{\mu(\delta, x^*)}(x^*, x) := \frac{\mu(\delta, x^*)}{2} \|Ax - y^\delta\|^2 + \frac{1}{2} \|x - x^*\|^2. \quad (7)$$

Since μ not only depends on x^* but also on δ via the equality

$$\|Ax - y^\delta\| = \delta, \quad (8)$$

we propose the following alternating algorithm:

0. Set an initial μ .
1. Solve $x(\mu) := \arg \min_{x \in X} L_\mu(x^*, x)$.
2. Adjust μ via Newton step on $\varphi(\mu) := \|Ax(\mu) - y^\delta\|^2 - \delta^2$.
3. Repeat 1. and 2. until some stopping criterion is reached.

To solve step 1. we can calculate

$$0 \stackrel{!}{=} F_\mu(x^*, x) := \partial_x L_\mu(x^*, x)^T = (\mathbb{1} + \mu A^T A) x - (\mu A^T y^\delta + x^*) \quad (9)$$

which leads to

$$x = (\mathbb{1} + \mu A^T A)^{-1} (\mu A^T y^\delta + x^*). \quad (10)$$

This can be nicely solved via the efficient conjugate gradient method (CG-method) (Hestenes and Stiefel [1952]), which does not have to calculate $A^T A$ or even hold it in memory. This can, especially for short-fat matrices (like used in compressed sensing (Eldar and Kutyniok [2012])), be a significant computational advantage.

To solve step 2. we need to calculate

$$\varphi'(\mu) = 2 (Ax - y^\delta)^T \partial_\mu x, \quad (11)$$

Algorithm 1: Projection of a point into the set of valid solutions

```

1 function Projection into Valid Solutions ( $A, y^\delta, \delta, x^*$ ):
   Input : Matrix  $A : X \rightarrow Y$ , vectors  $y^\delta \in Y$ ,  $x^* \in X$  and scalar  $\delta > 0$ 
   Output :  $\arg \min_{x \in X} \|x - x^*\|$  s.t.  $\|Ax - y^\delta\| = \delta$ 
2  $\mu \leftarrow \frac{\|x^*\|}{10\|A\|\delta}$  // Empirical guess, loosely motivated by  $0 = F_\mu(x^*, x)$ .
3 while not converged do
4    $x \leftarrow M^{-1}(x^* + \mu A^T y^\delta)$ 
5    $\mu \leftarrow \mu - \frac{\varphi(\mu)}{\varphi'(\mu)}$ 
6 end
7 return  $x$ 

```

where we can set $M := \mathbb{1} + \mu A^T A$ and use

$$0 = \partial_\mu (M^{-1}M) = \partial_\mu (M^{-1})M + M^{-1}\partial_\mu M \Rightarrow \partial_\mu M^{-1} = -M^{-1}\partial_\mu M M^{-1} \quad (12)$$

to calculate

$$\begin{aligned}
\partial_\mu x &= \partial_\mu \left((\mathbb{1} + \mu A^T A)^{-1} (\mu A^T y^\delta + x^*) \right) \\
&= \partial_\mu (M^{-1}x^* + \mu M^{-1}A^T y^\delta) \\
&= \partial_\mu (M^{-1})x^* + M^{-1}A^T y^\delta + \mu \partial_\mu (M^{-1})A^T y^\delta \\
&= \partial_\mu (M^{-1})x^* + M^{-1}A^T y^\delta + \mu \partial_\mu (M^{-1})A^T y^\delta \\
&= M^{-1} [-A^T A M^{-1}x^* + A^T y^\delta - \mu A^T A M^{-1}A^T y^\delta].
\end{aligned}$$

Also all these applications of M^{-1} can efficiently be calculated with the CG-method. The above calculations can be used to flesh out the projection algorithm in more detail, see Algorithm 1. In practice we stop the computation for $|\|y^\delta - Ax^\dagger\| - \delta|$ being $\leq 10^{-6}$, where x^\dagger the current reconstruction. For a complexity analysis of the algorithm see Figure 15 in the appendix.

The algorithm allows us, given the projection P_U , to solve the inverse problem in the sense of finding a valid and plausible solution via Expression (2).

To use P_U as a layer in a neural network and to incorporate it in a backpropagation training process we have to be able to calculate its derivative. As already mentioned, using automatic differentiation may not be feasible, due to the possibility huge memory requirements caused by the iterative nature of Algorithm 1 (since this effectively would have to be realized via several subsequent layers).

To overcome this problem we now utilize the implicit function theorem (Krantz and Parks [2012]) to calculate the derivative of P_V in a way that is also agnostic of the specific algorithm used to calculate the projection itself. This allows the backpropagation procedure to ignore the inner calculations of P_V and treat it essentially as a black box procedure. To be more specific, given x^* and $x := P_V x^*$, we want to calculate $\partial_{x^*} x$.

Since, due to Expression (9), we have

$$0 = F_\mu(x^*, x) := (\mathbb{1} + \mu A^T A)x - (\mu A^T y^\delta + x^*) \quad (13)$$

$$= \mu (A^T Ax - A^T y^\delta) + x - x^*, \quad (14)$$

we can calculate the relevant μ via

$$\mu = \|x - x^*\| / \|A^T (Ax - y^\delta)\|, \quad (15)$$

completely agnostic of the specific algorithm used in the forward propagation to calculate P_V .

We can now use the implicit function theorem and, considering Expression (14), obtain

$$\partial_{x^*} x = -(\partial_x F_\mu)^{-1} \partial_{x^*} F_\mu = (\partial_x F_\mu)^{-1} = (\mathbb{1} + \mu A^T A)^{-1} = (\partial_{x^*} x)^T. \quad (16)$$

We are now able to calculate $(\partial_{x^*} x)^T g^T$, which is necessary of the backpropagation, where g is the gradient flowing downwards from the layer above again – like in Algorithm 1 – this can be done efficiently via the CG-method, since $(\partial_{x^*} x)^T$ is symmetric and positively definite.

This allows us to implement P_U as a layer in an end-to-end trainable network. We provide code for a PyTorch (Paszke et al. [2017]) implementation of the projection layer, see Anonymous [2019].

2.4 Interpretation

In this subsection we discuss interpretations of the PM and its parts and how it relates to variations of the classical L_2 -regularization

$$x_{L_2}(\mu) := \arg \min_x \frac{\mu}{2} \|Ax - y^\delta\|^2 + \|Lx\|^2, \quad (17)$$

for some regularization parameter $\mu > 0$ and some linear continuous operator L , often simply $L = id$ (Engl et al. [1996]).

We start by interpreting P_V in the L_2 context. Usually the regularization parameter μ is chosen according to the Morozov's Discrepancy Principle (Morozov [2012]), which, in its classical form states that μ should be chosen such that (Scherzer [1993])

$$\|Ax_{L_2}(\mu) - y^\delta\| = \delta. \quad (18)$$

This leads to the nice interpretation that, for $L = \mathbb{1}$, we have

$$P_V 0 = x_{L_2}(\mu(\delta, 0)), \quad (19)$$

i.e. μ is *chosen according to Morozov*.

A further similarity to the L_2 -regularization becomes apparent, when stating the PM via the expression

$$x_{k+1} := \arg \min_x \frac{\mu(\delta, P_U(x_k))}{2} \|Ax - y^\delta\|^2 + \frac{1}{2} \|x - P_U(x_k)\|^2, \quad (20)$$

where $x_0 = 0$. This looks similar to a non-linear version of the non-stationary iterated Tikhonov regularization which is given via

$$x_{k+1} := \arg \min_x \frac{\mu_k}{2} \|Ax - y^\delta\|^2 + \frac{1}{2} \|Lx - Lx_k\|^2, \quad (21)$$

where also $x_0 = 0$ and $\{\mu_k\}_k$ some predetermined sequence (Hank and Groetsch [1998]).

3 Relation to Regularization by Denoising (RED)

In this section we want to discuss the connection of the PM with Regularization by Denoising (RED) (Romano et al. [2017]). It could be argued, that the RED (as a direct “descendent” of Plug-and-Play priors (Venkatakrishnan et al. [2013])) and Deep Image Prior (DIP), which we discuss in Section 4, are two of the most relevant recent approaches to regularization.

RED is given by the minimization of the somewhat strange, for technical reasons chosen, functional

$$L_{\text{RED}}(\mu) = \frac{\mu}{2} \|Ax - y^\delta\|^2 + x^T (x - f(x)), \quad (22)$$

where f is an arbitrary denoiser such that

- f is (locally) positively homogeneous of degree 1, i.e. $f(cx) = cf(x)$ for $c \geq 0$ and
- f is strongly passive, i.e. the spectral radius of $\partial_x f(x) \leq 1$.

Both of these properties one associates with linear projections.

An algorithm to solve the minimization problem is given in Romano et al. [2017] and can be expressed via

$$x_{k+1} := \arg \min_x \frac{\mu}{2} \|Ax - y^\delta\|^2 + \frac{1}{2} \|x - f(x_k)\|^2, \quad (23)$$

for an initial $x_0 = 0$ and some fixed $\mu > 0$.

This means that, if we associate f with P_U , RED as stated in Expression (23), can be seen as a relaxation (setting μ constant) of the PM, as stated in Expression (20).

We compared RED and PM of the course of the reconstruction process, see Figure 1, where we use the BM3D denoiser (Dabov et al. [2006]) as f and as an approximation for P_U . For our numerical experiments we set A to be the (underdetermined) Radon transform (Helgason and Helgason [1999])

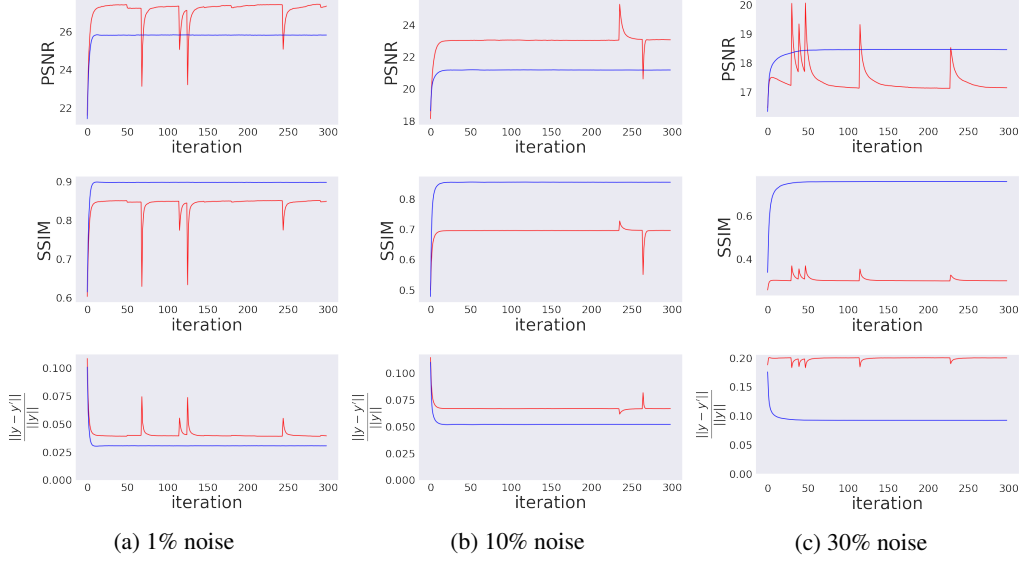
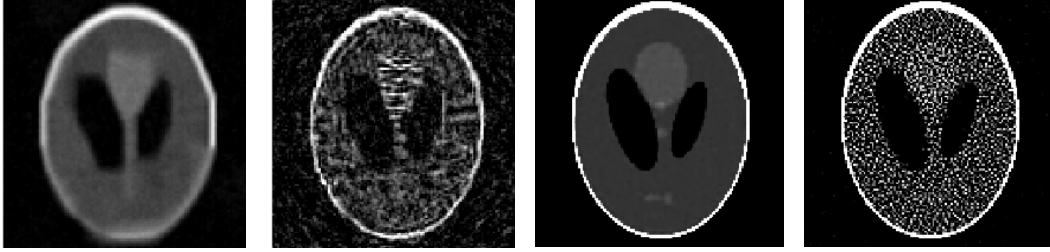


Figure 1: The behavior of RED (red) and the PM (blue) over the course of 300 iterations for reconstructions at three different noise levels. We compare the PSNR, SSIM and $\frac{\|y - y'\|}{\|y\|}$, where $y = Ax$ is the noise free measurement of the ground truth and $y' = Ax^\dagger$ is the noise free measurement of the reconstruction.



(a) PM with a PSNR of 18.45 and a SSIM of 0.76. (b) RED with a PSNR of 0.76 and a SSIM of 0.3. (a) DIP+ δ with a PSNR of 39.29 and a SSIM of 0.99. (b) DIP with a PSNR of 14.74 and a SSIM of 0.62.

Figure 2: The last PM and RED reconstructions for a noise level of 30% Figure 3: The last DIP+ δ and DIP reconstructions for a noise level of 1%

with 30 angles, use the classical Shepp-Logan phantom (Shepp and Logan [1974]) as the ground truth x and set our noise level δ to 1%, 10% and 30% of the norm of $y = Ax$. We ran each of the experiment 10 times (different noise), with similar results to the ones shown in Figure 1. We see that the PM does not outperform RED for all noise levels in the Peak signal-to-noise ratio (PSNR), but in the Structural Similarity Index (SSIM) and also in the L_2 error of Ax vs Ax^\dagger , where x^\dagger the reconstruction. Additionally the reconstruction process runs smoother for the PM than for RED and does not seem to degrade at high noise levels over time. The regularization parameter for RED were determined via an exponential line search for the best final reconstruction. The PM required no parameter. The 300 iterations for RED and for the PM took both on the order of one hour on an Intel i7 CPU with 2.6GHz. You can find the last reconstructions for a noise level of 30% in Figure 2 and comprehensive comparison of reconstructions in in the appendix, Figure 9, 10 and 11.

4 Application to Deep Image Prior (DIP)

In this section we discuss how one can implement the central idea of finding an element in $U \cap V$ for the case where U is given by all possible reconstructions from a Deep Image Prior (DIP).

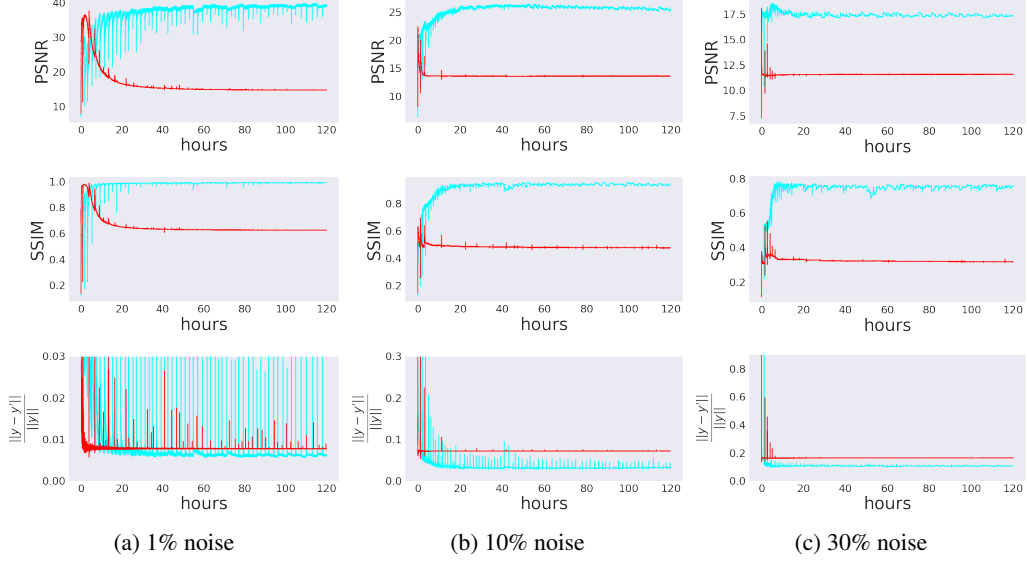


Figure 4: The behavior of the minimization of L_{DIP} (red) and of $L_{\text{DIP}+\delta}$ (cyan) over the course of the reconstruction.

The idea of using DIP to solve inverse problems, as described by Veen et al. [2018], is to minimize the functional

$$L_{\text{DIP}}(\Theta) := \frac{1}{2} \|AG_{\Theta}(z) - y^{\delta}\|^2 \quad (24)$$

with regard to Θ , where $G_{\Theta}(z)$ is an untrained neural network with a fixed random input z and parameters Θ . The reconstruction is then given via $G_{\Theta}(z)$, i.e. the output of the network.

We propose the following simple modification to the DIP functional based on the idea to find a valid and plausible reconstruction. Specifically we propose

$$L_{\text{DIP}+\delta}(\Theta) := (\|AG_{\Theta}(z) - y^{\delta}\|^2 - \delta^2)^2. \quad (25)$$

Here the reconstruction is given by $G_{\Theta}(z)$ after the minimization.

We now numerically compare this modified functional $L_{\text{DIP}+\delta}$ with L_{DIP} in the same setup as used in Section 3 for RED and the PM based on BM3D. As the DIP network we use the “skip net” UNet described in the original DIP paper (Ulyanov et al. [2018]) and Adam (Kingma and Ba [2014]) with standard settings (of PyTorch), which we found to work best for the DIP reconstructions. The results can be found in Figure 4. Like in Section 3 we compare the PSNR, SSIM and $\|y - y'\|/\|y\|$, where $y = Ax$ is the noise free measurement of the ground truth and $y' = Ax^{\dagger}$ the noise free measurement of the reconstruction. We plot the reconstruction over time, not over the number of iterations, to clearly show that even over relatively long time scales the solutions of $L_{\text{DIP}+\delta}$ do not exhibit signs of much deterioration. We ran the experiments in parallel on two Nvidia GeForce GTX 1080 ti. You can find the last reconstructions for a noise level of 1% in Figure 3 and comprehensive comparison of reconstructions in the appendix, Figure 12, 13 and 14. All experiments reached approximately 750,000 iterations over the course of the 120 hours of the experiment. We find that the modified functional shows much less deterioration of the reconstruction overtime and outperforms the vanilla DIP (except for short spikes) in all our metrics.

5 von Neumann Projection Architecture

In this section we discuss how one can learn, in an end-to-end fashion, a replacement for P_U , where U an arbitrary set. For this we heavily rely on the fact that we can calculate the gradients of P_U and can therefore use it as a layer (see Section 2.3).

Based on Expression (2) we propose the following neural network architecture:

$$G_{\theta}(A, y^{\delta}, \delta, x_0) := P_{V(A, y^{\delta}, \delta)} \circ g_{\theta, n-1} \circ P_{V(A, y^{\delta}, \delta)} \circ \dots \circ g_{\theta, 0} \circ P_{V(A, y^{\delta}, \delta)}(x_0), \quad (26)$$

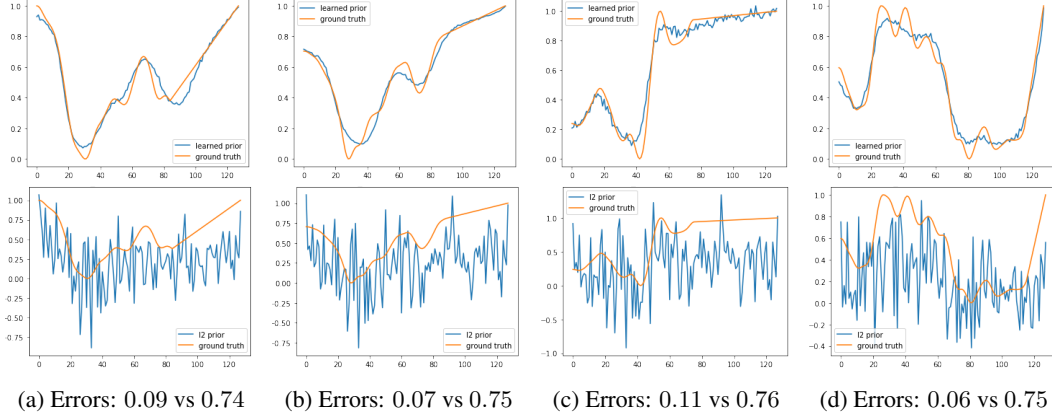


Figure 5: Learned (top) v.s. best mean-squared-error l_2 -reconstructions (bottom) with there respective relative l_2 -errors, i.e. $\frac{\|x - x_{\text{reconstruction}}\|}{\|x\|}$.

where the $g_{\theta,i} : X \rightarrow X$ are neural networks, e.g. UNets (Ronneberger et al. [2015]) or autoencoders (Ng [2011]), for simplicity we set $x_0 = 0$.

This type of alternating architecture, which we call **von Neumann projection architecture** (vNPA), allows one to use the PM, while incorporating prior information from data in a highly customized manner. This is in stark contrast to the use of usually quite general Plug-and-Play priors (Venkatakrishnan et al. [2013], Sreehari et al. [2016]), which are not specifically adapted to the reconstruction task. Unlike other end-to-end approaches this architecture, using P_V , guarantees the data consistency of the reconstruction.

We now demonstrate the approach on a toy example. For that we set U to be a set of low frequency functions $f : [0, 127] \ni x \mapsto f(x) \in [0, 1]$, which for some random $x \geq 63$ turn continuously into linear functions such that $f(127) = 1$, see Figure 8 in the appendix for example plots and Python code that creates random instances of these functions in the form of vectors of the length 128. One could try to design a handcrafted prior for these arbitrarily chosen functions, but it would be easier to simply learn one. As the forward operator, $A \in \mathbb{R}^{64 \times 128}$, we use a typical compressed sensing operator i.e. the entries are samples from a standard Gaussian distribution.

We use the vNPA as described in Expression (26), with $n = 4$. Each $g_{\theta,i}$ is a separate vanilla autoencoder with the widths $128 \rightarrow 64 \rightarrow 32 \rightarrow 64 \rightarrow 128$, where all layers up to the last one are vanilla ReLU layer, the last one being a vanilla Sigmoid layer. We trained it with a batch size of 32 and Adam (Kingma and Ba [2014]) at learning rate of 10^{-4} for 20,000 batches over the course of three hours on an Nvidia GeForce GTX 960M.

Example reconstructions via the network compared to L_2 reconstructions (the regularization parameter optimized such that it minimizes the L_2 error to the ground truth) can be found in Figure 5. Each took less than half a second to compute. The network produces clearly better reconstruction than the optimized L_2 regularization.

6 Conclusion

We proposed a projectional approach of optimizing for an element that is valid and plausible given the operator, measurement and noise level. We find that the approach is fruitful and widely applicable. Specifically we demonstrated its applicability on the one hand via very general Plug-and-Play priors like BM3D and DIP and on the other hand via highly task specific learned priors via the von Neumann projection architecture.

We also show how the approach can be connected to the well studied iterated Tikhonov reconstructions, how it allows for an interpretation of the somewhat strange, but highly effective RED functional and how it can be used to stabilize and improve DIP reconstructions.

References

- J. Adler and O. Öktem. Learned primal-dual reconstruction. *IEEE transactions on medical imaging*, 2018.
- Anonymous. Projection layer implementation, 2019.
- H. H. Bauschke and J. M. Borwein. On the convergence of von neumann’s alternating projection algorithm for two sets. *Set-Valued Analysis*, 1993.
- A. Bora, A. Jalal, E. Price, and A. G. Dimakis. Compressed sensing using generative models. In *Proceedings of the 34th International Conference on Machine Learning-Volume 70*. JMLR. org, 2017.
- K. Dabov, A. Foi, V. Katkovnik, and K. Egiazarian. Image denoising with block-matching and 3d filtering. In *Image Processing: Algorithms and Systems, Neural Networks, and Machine Learning*. International Society for Optics and Photonics, 2006.
- S. Dittmer, T. Kluth, P. Maass, and D. Oterio Baguer. Regularization by architecture: A deep prior approach for inverse problems. *arXiv preprint arXiv:1812.03889*, 2018.
- D. Drusvyatskiy, A. D. Ioffe, and A. D. Lewis. Transversality and alternating projections for nonconvex sets. *Foundations of Computational Mathematics*, 2015.
- Y. C. Eldar and G. Kutyniok. *Compressed sensing: theory and applications*. Cambridge University Press, 2012.
- H. W. Engl, M. Hanke, and A. Neubauer. *Regularization of inverse problems*. Springer Science & Business Media, 1996.
- L. G. Gubin, B. T. Polyak, and E. V. Raik. The method of projections for finding the common point of convex sets. *USSR Computational Mathematics and Mathematical Physics*, 1967.
- M. Hank and C. W. Groetsch. Nonstationary iterated tikhonov regularization. *Journal of Optimization Theory and Applications*, 1998.
- A. Hauptmann, F. Lucka, M. Betcke, N. Huynh, J. Adler, B. Cox, P. Beard, S. Ourselin, and S. Arridge. Model-based learning for accelerated, limited-view 3-d photoacoustic tomography. *IEEE transactions on medical imaging*, 2018.
- M. T. Heath. *Scientific computing: an introductory survey*. SIAM, 2018.
- S. Helgason and S. Helgason. *The radon transform*. Springer, 1999.
- M. R. Hestenes and E. Stiefel. *Methods of conjugate gradients for solving linear systems*. NBS Washington, DC, 1952.
- D. P. Kingma and J. Ba. Adam: A method for stochastic optimization. *arXiv preprint arXiv:1412.6980*, 2014.
- S. G. Krantz and H. R. Parks. *The implicit function theorem: history, theory, and applications*. Springer Science & Business Media, 2012.
- A. S. Lewis and J. Malick. Alternating projections on manifolds. *Mathematics of Operations Research*, 2008.
- A. S. Lewis, D. R. Luke, and J. Malick. Local linear convergence for alternating and averaged nonconvex projections. *Foundations of Computational Mathematics*, 2009.
- S. Lunz, C. Schoenlieb, and O. Öktem. Adversarial regularizers in inverse problems. In *Advances in Neural Information Processing Systems*, 2018.
- G. Mataev, M. Elad, and P. Milanfar. Deepred: Deep image prior powered by red. *arXiv preprint arXiv:1903.10176*, 2019.

- V. A. Morozov. *Methods for solving incorrectly posed problems*. Springer Science & Business Media, 2012.
- A. Ng. Sparse autoencoder. *CS294A Lecture notes*, 2011.
- A. Paszke, S. Gross, S. Chintala, G. Chanan, E. Yang, Z. DeVito, Z. Lin, A. Desmaison, A. Luca, and A. Lerer. Automatic differentiation in PyTorch. In *NIPS Autodiff Workshop*, 2017.
- Y. Romano, M. Elad, and P. Milanfar. The little engine that could: Regularization by denoising (red). *SIAM Journal on Imaging Sciences*, 2017.
- O. Ronneberger, P. Fischer, and T. Brox. U-net: Convolutional networks for biomedical image segmentation. In *International Conference on Medical image computing and computer-assisted intervention*. Springer, 2015.
- Y. Saad. *Iterative methods for sparse linear systems*. siam, 2003.
- O. Scherzer. The use of morozov’s discrepancy principle for tikhonov regularization for solving nonlinear ill-posed problems. *Computing*, 1993.
- L. A. Shepp and B. F. Logan. The fourier reconstruction of a head section. *IEEE Transactions on nuclear science*, 1974.
- S. Sreehari, S. V. Venkatakrishnan, B. Wohlberg, G. T. Buzzard, L. F. Drummy, J. P. Simmons, and C. A. Bouman. Plug-and-play priors for bright field electron tomography and sparse interpolation. *IEEE Transactions on Computational Imaging*, 2016.
- M. Talagrand. A new look at independence. *The Annals of probability*, 1996.
- D. Ulyanov, A. Vedaldi, and V. Lempitsky. Deep image prior. In *Proceedings of the IEEE Conference on Computer Vision and Pattern Recognition*, 2018.
- D. Van Veen, A. Jalal, E. Price, S. Vishwanath, and A. G. Dimakis. Compressed sensing with deep image prior and learned regularization. *arXiv preprint arXiv:1806.06438*, 2018.
- S. V. Venkatakrishnan, C. A. Bouman B., and Wohlberg. Plug-and-play priors for model based reconstruction. In *2013 IEEE Global Conference on Signal and Information Processing*. IEEE, 2013.
- G. Yang, S. Yu, H. Dong, G. Slabaugh, P. L. Dragotti, X. Ye, F. Liu, S. Arridge, J. Keegan, and Y. Guo. Dagan: deep de-aliasing generative adversarial networks for fast compressed sensing mri reconstruction. *IEEE transactions on medical imaging*, 2018.

Appendix

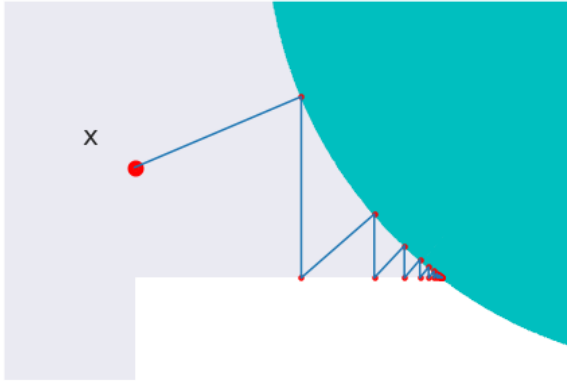


Figure 6: A visualization of von Neumann's projection algorithm: mapping the point x onto the intersection of a disk (cyan) and a square (white).

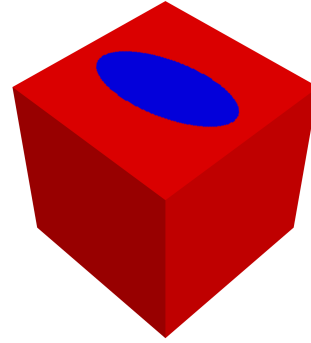
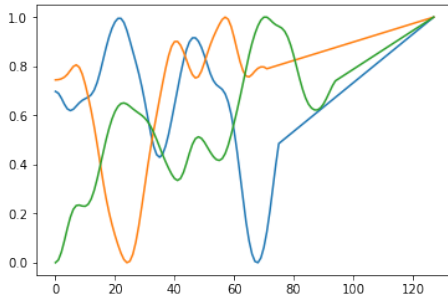


Figure 7: The elliptic cylinder \bar{V} (blue) within the space X (red) for the finite dimensional case $\text{rank}(A) = 2$ and $\dim(X) = 3$.



```
import numpy as np

def get_function_sample(function_length=128):
    # Create random frequency amplitudes
    freq = np.random.normal(0, 1, function_length + 1)
    # Dampen higher frequencies
    freq *= np.logspace(0, -8, function_length + 1)
    # apply inverse real Fourier transform
    f = np.fft.irfft(freq)
    # Remove symmetric part
    f = f[:function_length]
    # Normalize between 0 and 1
    f -= np.min(f)
    f /= np.max(f)

    # Generate random point to begin linear part
    start_lin = int(np.random.rand() * 64 + 64)
    # Generate linear part
    f[start_lin:] = np.linspace(f[start_lin], 1, len(f[start_lin:]))

    return f
```

Figure 8: Three example test functions and the Python code that creates one.

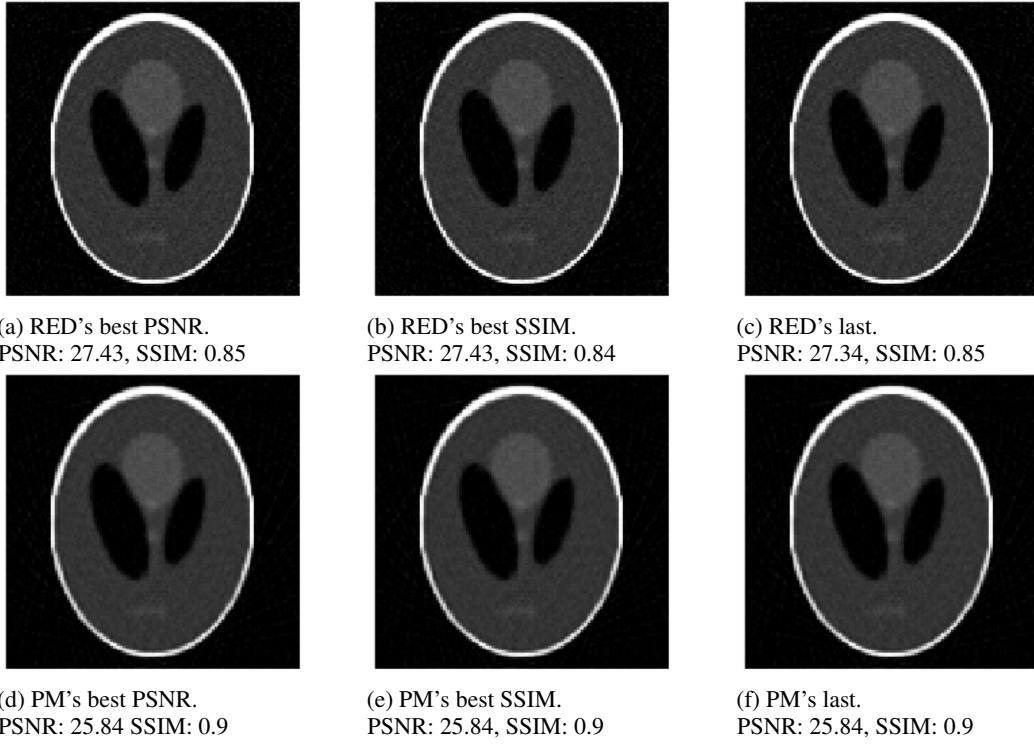


Figure 9: RED and PM reconstructions at 1% noise.

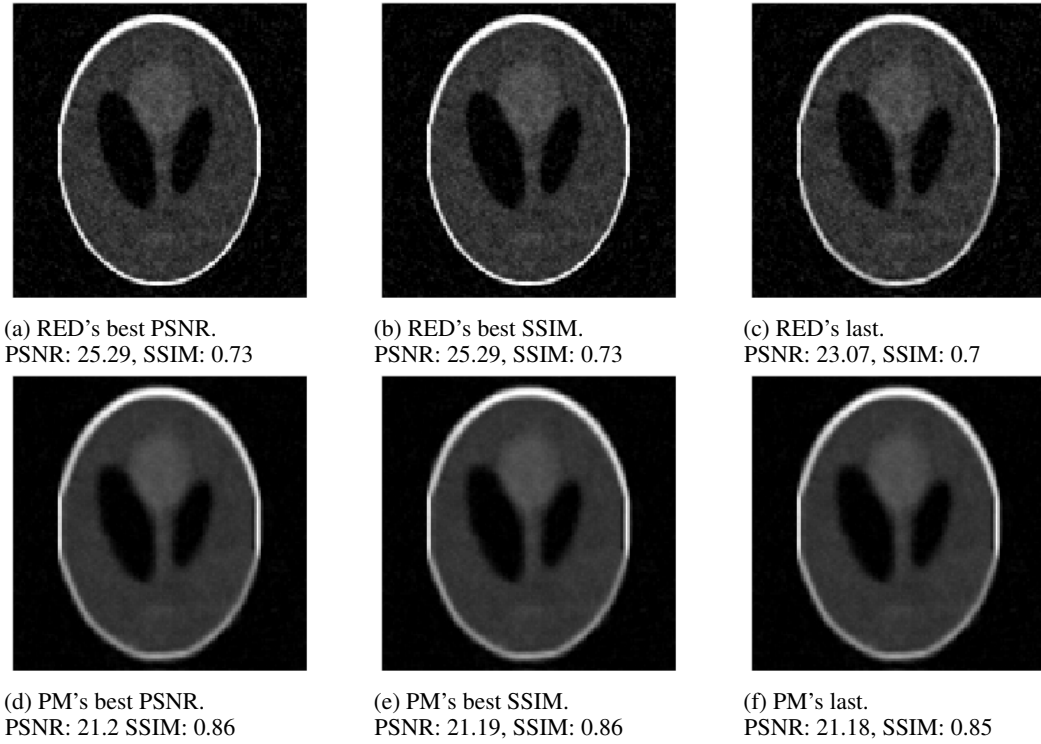


Figure 10: RED and PM reconstructions at 10% noise.

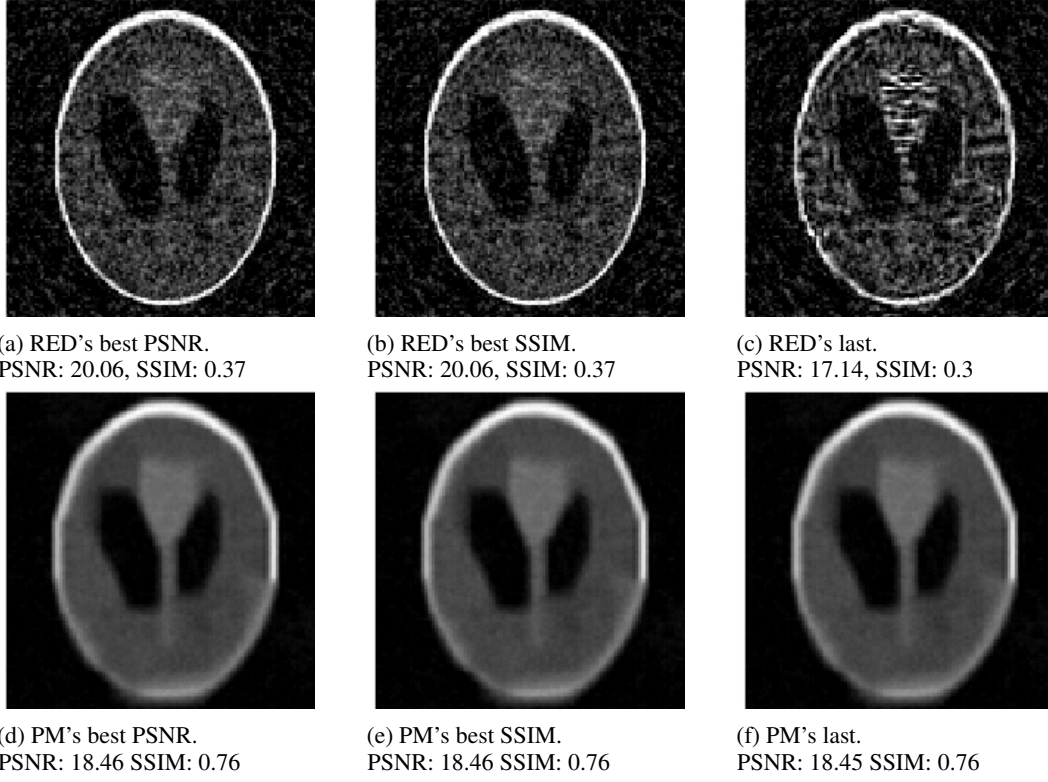


Figure 11: RED and PM reconstructions at 30% noise.

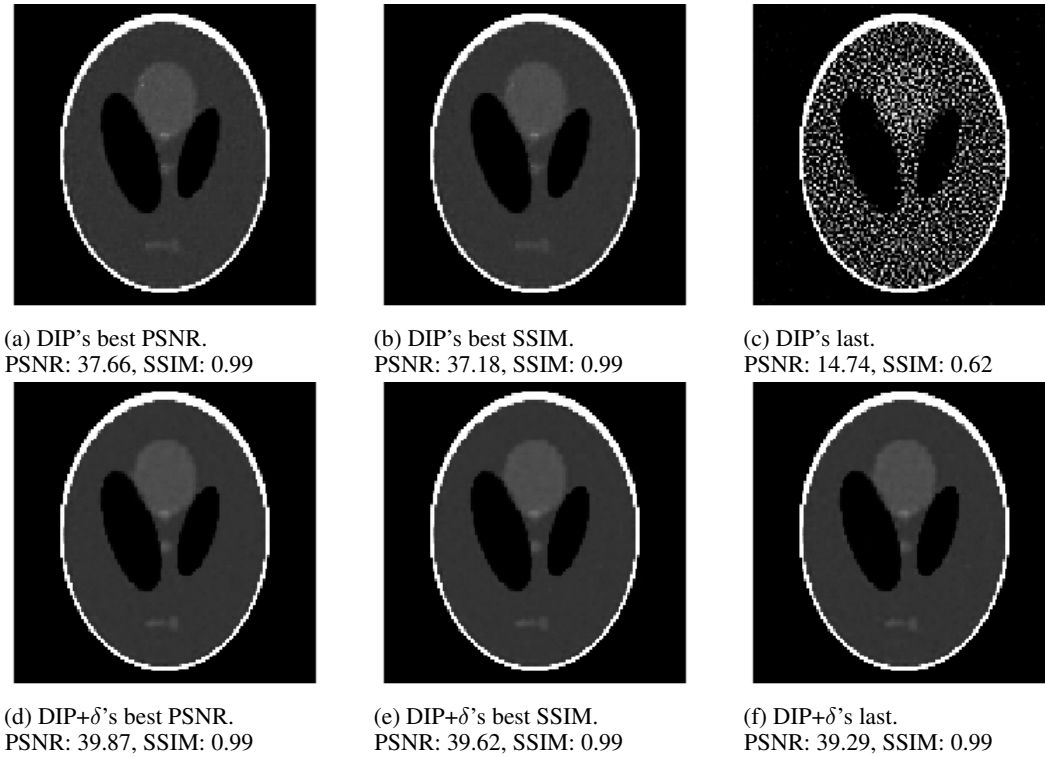


Figure 12: DIP and DIP+ δ reconstructions at 1% noise.

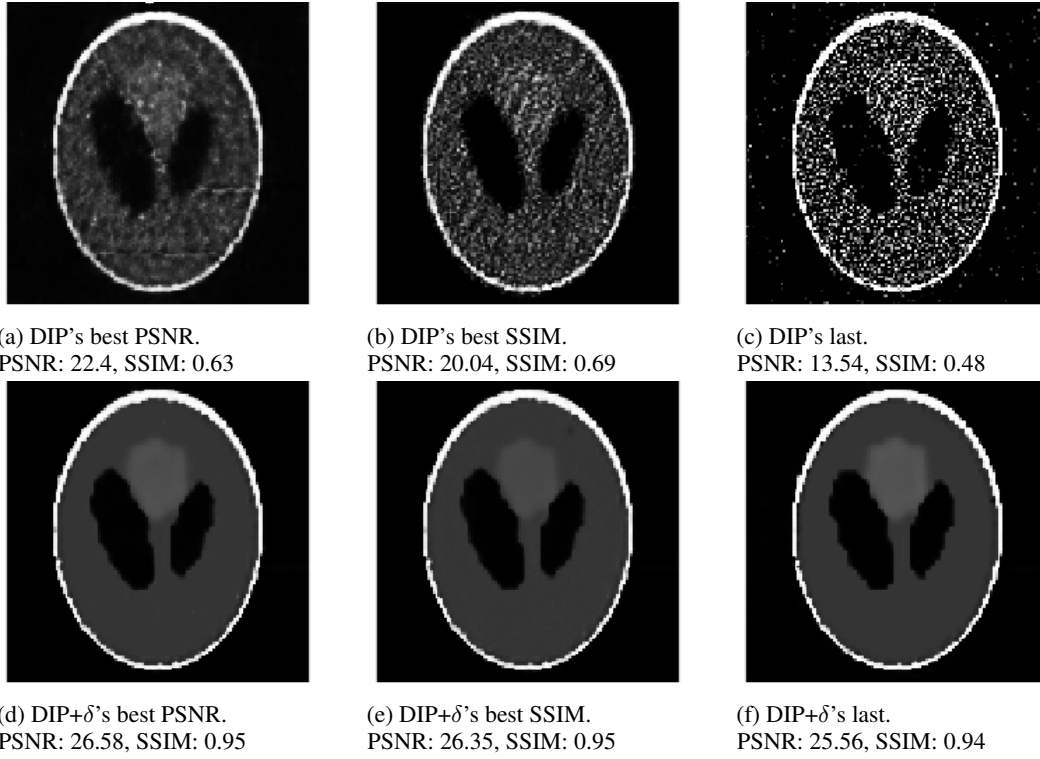


Figure 13: DIP and DIP+ δ reconstructions at 10% noise.

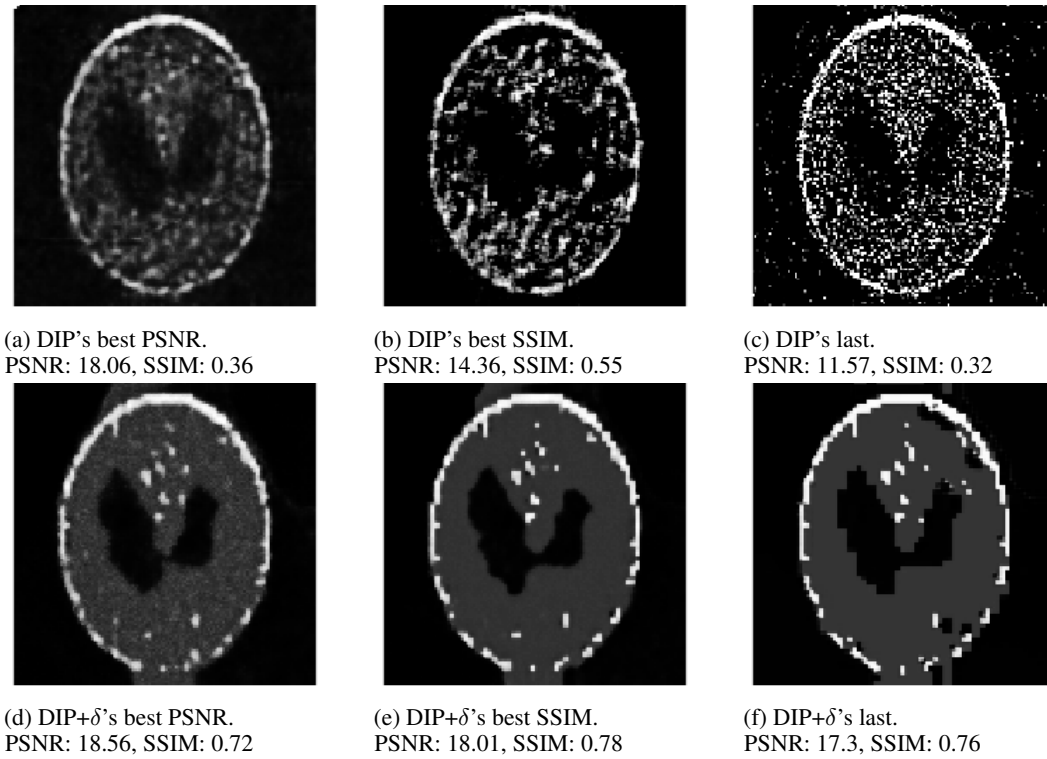


Figure 14: DIP and DIP+ δ reconstructions at 30% noise.

The complexity of Algorithm 1, can simply be estimated via the complexity of the Newton method, $O(\log \frac{1}{\epsilon} F(\frac{1}{\epsilon}))$ (Heath [2018]), where $\epsilon > 0$ is the required precision and F is the complexity of the CG-method applied to M . Assuming κ is the condition number of M the complexity of the CG-method is $O(\sqrt{\kappa} \log \frac{1}{\epsilon})$ (Saad [2003]). This results in an overall complexity of

$$O\left(\sqrt{\kappa} \left(\log \frac{1}{\epsilon}\right)^2\right). \quad (27)$$

Figure 15: A complexity analysis of Algorithm 1.